Int. J. Electrochem. Sci., 12 **(2017)** 9084 – 9093, doi: 10.20964/2017.10.60

International Journal of
ELECTROCHEMICAL
SCIENCE
www.electrochemsci.org

Bio-Synthesis of $LiFePO_4$/C composites for lithium ion battery

Yue Cao[1,2], *Wangjun Feng*[1,2], *Wenxiao Su*[2]

[1] State Key Laboratory of Advanced Processing and Recycling Nonferrous Metals, Lanzhou University of Technology, Lanzhou 730050, China
[2] School of Science, Lanzhou University of Technology, Lanzhou 730050, China
*E-mail: wjfeng@lut.cn

Received: 6 July 2017 / *Accepted:* 9 August 2017 / *Published:* 12 September 2017

According to the biomineralization assembly concept, high-performance $LiFePO_4$/C composites are successfully obtained via an effective and controllable biomimetic sol-gel method. The key step of this method is using the Baker's yeast cells as structural templates and biocarbon sources. The phase identification of four different $LiFePO_4$/C composites are tested by X-ray diffraction (XRD), scanning electron microscopy (SEM) and transmission electron microscopy (TEM), which are used to research the morphology, size and structure of $LiFePO_4$/C composites. And the electrochemical performance tests demonstrate when the amount of Baker's yeast cells are 20g L^{-1}, $LiFePO_4$/C composites exhibit the best discharge specific capacity, 151.6mAh g^{-1} at 0.1C, which is higher than the pristine $LiFePO_4$ electrode (116.8mAh g^{-1} at 0.1C) without Baker's yeast cells. After 50 cycles at 0.1C, the discharge capacity maintains 147.8mAh g^{-1} (97.5% of its initial value). Also, the sample $LiFePO_4$/C with 20 g L^{-1} yeast cells shows a couple of redox peaks between 3.34V to 3.53V which is narrower and incisive, and the resistance is much smaller than other samples. Therefore the $LiFePO_4$/C composites synthesized by yeast cells are an ideal type of cathode-active material for lithium ion batteries.

Keywords: $LiFePO_4$/C composites, yeast cells, biocarbon, electrochemical performance

1. INTRODUCTION

In recently years, lithium ion battery has been used as alternative energy sources for mobile electronic devices, electrical vehicles (EVs) and hybrid electrical vehicles (HEVs) [1–3]. Currently, because of low cost without noble element, good electrochemical stability, flat voltage profile (3.4V), large theoretical specific capacity (170mAh g^{-1}), especially an excellent safety performance [4-7], a considerable amount of resources are devoted to optimize the performance of lithium ion batteries [8-11]. And the olivine $LiFePO_4$ seems to be one of the most hopeful cathode materials for lithium ion battery [12, 13]. However, the drawbacks include extremely low electronic conductivity (~10^{-9} S cm^{-1})

and Li^+ conductivity (~1.8×10^{-14} cm^2 s^{-1}), which can result in poor electrochemical properties and hinder the commercial production of $LiFePO_4$ [14]. To solve these drawbacks, a large number of efforts have been directed towards modifying the crystal structure and morphology [15, 16], reducing the size of $LiFePO_4$ particles [17], or creating layers to increase the electronic conductivity and decrease the Li^+ diffusion resistance [18, 19].

In the past decade, many effects researches have been done to overcome the disadvantages of low electronic conductivity and Li^+ conductivity for $LiFePO_4$ materials. The reducing of particle size to a nanoscale dimension and carbon coating are the most widely used strategies to enhance lithium ion diffusivity and increase electronic conductivity for the potential active materials. However, it is difficult to improve effectively and prepare simply via the traditional methods. Although some carbon coating $LiFePO_4$ composites or nanoscale $LiFePO_4$ materials had been obtained, the results are not perfect and the cost is too much. Aimed at this problem, many researchers have invented a method, by which they can prepare superior materials with yeast cells as biotemplates under ordinary conditions [20, 21] Du et al. [22] synthesized $Li_3V_2(PO_4)_3$/C microspheres using Baker's yeast cells, which show a good discharge capacity (126.7mAh g^{-1} at 0.2C) and large Li^+ diffusion coefficient. Hereafter, Chang et al. [23] had synthesized hierarchical mesoporous TiO_2 and mesoporous ZrP_2O_7 by Baker's yeast cells as biotemplates. In addition, a mesoporous $LiFePO_4$/C nanocomposite microsphere had been obtained by Wen He [24], which exhibits a well-proportioned size distribution (4.76μm), high tap density (1.74g cm^{-3}) and a large specific surface area (203m^2 g^{-1}). Based on aforementioned results, it can be agreed that Baker's yeast cells could be considered as an appropriate complete to composite $LiFePO_4$.

Herein, we report our results for $LiFePO_4$/C composites which were prepared by a bio-synthesis approach using Baker's yeast cells as structural templates and carbon sources. The synthesis, characterization and electrochemical behavior of $LiFePO_4$/C composites showed that the material have a nano-particle size and homogeneous carbon coating layer.

2. EXPERIMENTAL SECTION

2.1 Material Preparation

The reagents used in the work were $Fe(NO_3)_3\cdot9H_2O$, $NH_2H_2PO_4$, $LiOH\cdot H_2O$, $C_6H_8O_7\cdot H_2O$, Glucose anhydrouse and yeast cells (dry yeast). The raw materials were prepared that the stoichiometric of $Fe(NO_3)_3\cdot9H_2O$, $NH_2H_2PO_4$ and $LiOH\cdot H_2O$ were 1:1:1 in mole. In a typical experimental procedure, quantitative instant dry yeast (0 g L^{-1}, 10 g L^{-1}, 20 g L^{-1}, 30 g L^{-1}) were cultivated in 100ml glucose aqueous solution and formed a uniform emulsion, respectively. Then, the yeast cell solution was obtained via centrifugation and washing several times with distilled water. Firstly, $Fe(NO_3)_3\cdot9H_2O$ was dissolved in 100ml purified water to cultivate yeast cells for stirring at room temperature. Secondly, the $NH_2H_2PO_4$, $LiOH\cdot H_2O$ and $C_6H_8O_7\cdot H_2O$ were dropped into the solution with magnetic stirring. Citric acid was used in this work as chelating reagent and reducing agent. Then, the solution were moved into water bath kettle with vigorous stirring for 5h at 80℃ till

the solution became gel. After that, the prepared gel precursors were dried at 120℃ for 24h. Now, the precursors ($LiFePO_4$/yeast-0g L^{-1}, $LiFePO_4$/yeast-10g L^{-1}, $LiFePO_4$/yeast-20g, L^{-1} $LiFePO_4$/yeast-30g L^{-1}) were obtained. Finally, the prepared powders were sintered in a nitrogen atmosphere with muffle furnace at 700℃ for 6h, and the $LiFePO_4$/C composites were obtained.

2.2 Characterization

The crystal phase of all the samples were characterized by powder XRD using Bruker D8 Advance diffractometer with Cu Kαradiation from 10º to 80º. SEM images of the samples were collected by a JSM-6700F system operated with accelerating voltage of 20 kV. TEM images were obtained with a JEM -2100F system operated at 200 kV. High-resolution transmission electron microscopy (HRTEM) was carried out on a Philips Tecnai 20U-TWIN microscope at 300 kV.

2.3 Electrochemical Analysis

Electrochemical properties of the obtained pellet samples were detected using CR2025 coin-type cells, and the lithium metal was used as the counter electrode. The mixture of the $LiFePO_4$/C composites, acetylene black and Polyvinylidene Fluoride were 80:10:10 at a weight ratio, which were added in N-methylpyrrolidone to constitute uniform slurry. The obtained slurry was coated on an aluminum foil, dried 10h in a vacuum oven at 120°C. The cells were assembled in a glove box filled with high-purity argon. The Land CT2001A battery test system (Wuhan, China) was used to test the charge-discharge capacities from 2.4 V to 4.3 V. The electrochemical impedance (EIS) and Cyclic voltammetry (CV) measurement were tested on Electrochemical workstation. EIS was also recorded with the frequency ranging from 100 kHz to 10 mHz. The voltage range of the CV measurements was 2.5-4.2V and the scanning rate was 0.1mV s^{-1}.

3. RESULTS AND DISSCUSSION

In order to study the influence of yeast cells on crystalline structure of synthesized samples, the XRD patterns of all $LiFePO_4$/C composites and pure $LiFePO_4$ are shown in Fig.1. The diffraction peaks of the pure $LiFePO_4$ (yeast-0g L^{-1}) become weaker and fluctuant, which shows that is not an excellent crystallinity. The diffraction peaks of all samples using different additional amount of yeast cells can be majorly assigned to orthorhombic olivine-type structure of pure phase $LiFePO_4$ (JCPDS NO.40-1499). The peaks of $LiFePO_4$/C composites demonstrate that all products have a good crystallinity, and no characteristic peaks from carbon and other elements are observed. The reason is that the high-energy phosphate groups that have negative charges in network structure of yeast cell are preferentially bonded with ferrous ion, meanwhile the high-energy phosphate groups are the most important contributor to the free energy barrier for iron phosphate biomineralization at natural

conditions [21]. There are superabundant addition of yeast cells (30g L^{-1}), which causes the diffraction peak position shifted a small angle. It may be indicative of increasing lattice strain.

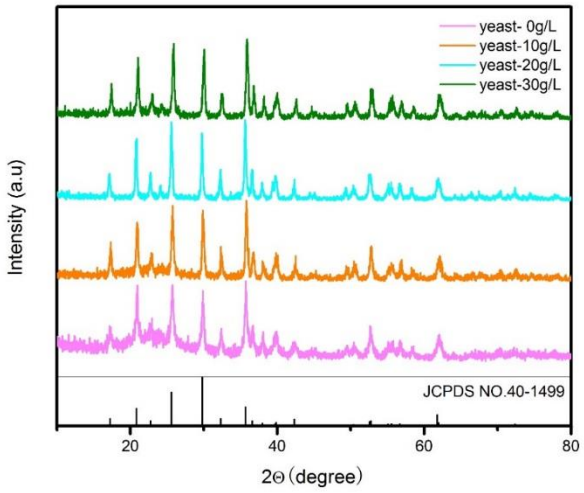

Figure 1. XRD patterns of various $LiFePO_4$/C at different additional amount of yeast cells

According to Scherrer formula and Bragg formula, the average crystalline size of all samples can be calculated from the full width at half maximum (FWHM). The corresponding parameters of the main diffraction peak of all samples are listed in Table 1. It can be found that unit cell volume is increasing with the addition of yeast cells except the $LiFePO_4$/yeast-30g L^{-1}. The reason may be the superabundant addition of yeast cells lead to the existence of lattice strain. So the calculative parameters matched up to the XRD patterns.

Table 1. The unit cell parameters of samples

sample	a(A^o)	b(A^o)	c(A^o)	Cell volume(A^3)
$LiFePO_4$/yeast- 0g L^{-1}	5.98667	10.31994	4.67812	289.02
$LiFePO_4$/yeast-10g L^{-1}	5.98474	10.33443	4.68272	289.62
$LiFePO_4$/yeast-20g L^{-1}	5.99323	10.32985	4.69195	290.48
$LiFePO_4$/yeast-30g L^{-1}	5.92919	10.05562	4.76202	283.92

The size, structure and morphology of the as-prepared products are presented by SEM. The yeast cells can be used as the structural templates and carbon sources during the process of annealing. Theoretically, carbon coating can effectively impede crystal and particle growth [25]. Fig.2a shows the SEM image of $LiFePO_4$/yeast-0g L^{-1}. It is obviously observed that many $LiFePO_4$ grains are aggregated about 1-2μm in diameter. $LiFePO_4$/C composites are composed of unique microsphere, which are achieved by biomineralization assembly assisted by yeast cells (Fig.2 b, c, d). When the additional amount of yeast cells are 10g L^{-1} (Fig.2 b), it only forms some trifling microspheres. The

reason is that the yeast cells are limited that a lot of $LiFePO_4$ particles do not appear self-assembly. However, the SEM image of Fig.2d ($LiFePO_4$/yeast-30g L^{-1}) shows there are many $LiFePO_4$ microspheres aggregated, because a larger amount of yeast cells are introduced excess carbon [26]. Fig.2c shows that the sample has a characteristic microspheric structure about 100-300nm, suggesting that the $LiFePO_4$/C nanoparticles are successfully obtained. In the image, the $LiFePO_4$/C composites have a simplex and homogeneous distribution.

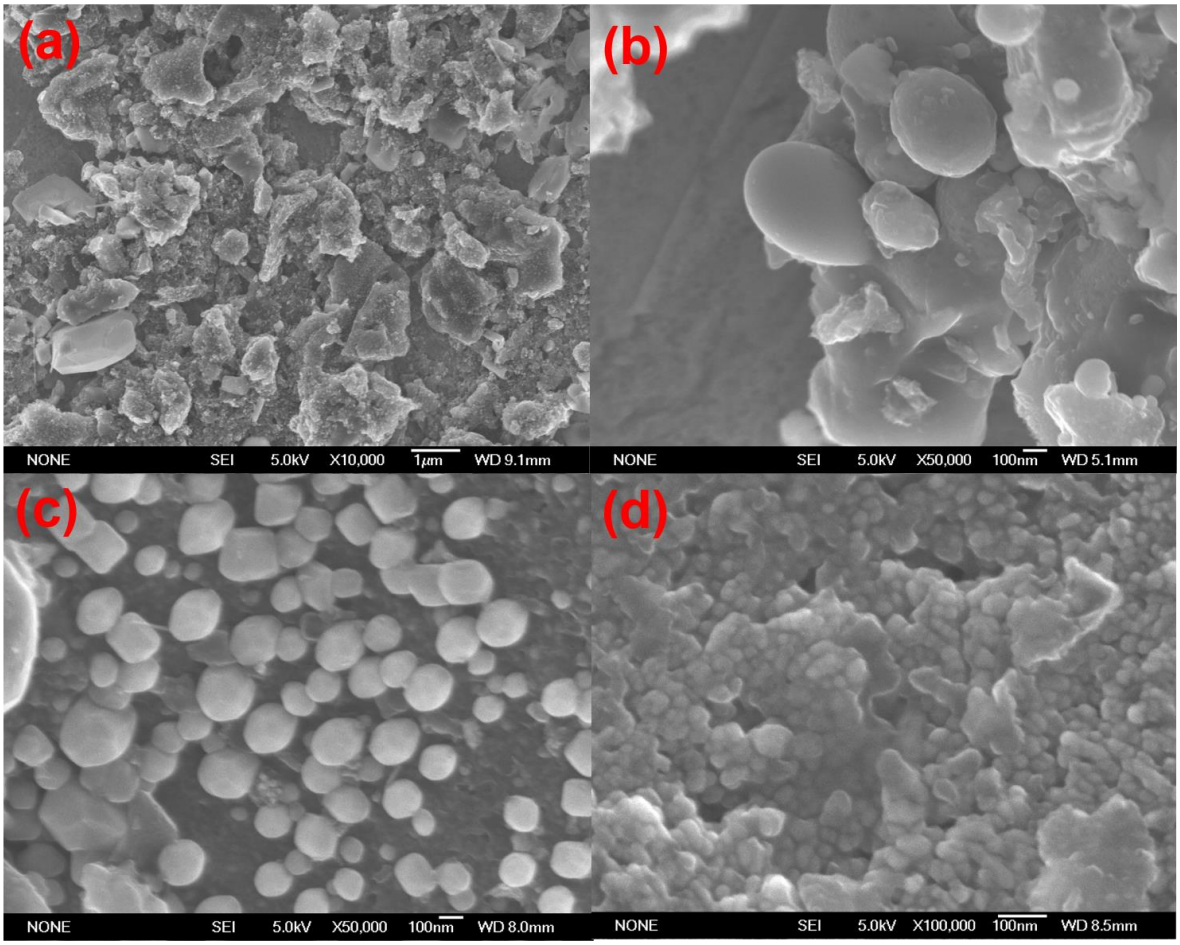

Figure 2. SEM images of all samples: (a) $LiFePO_4$/yeast-0g L^{-1}, (b) $LiFePO_4$/yeast-10g L^{-1}, (c) $LiFePO_4$/yeast-20g L^{-1}, (d) $LiFePO_4$/yeast-30g L^{-1}

EDS spectra image is obtained to illustrate element component of $LiFePO_4$/C nanoparticles (Fig.3.) [27]. This image is closely matched with the corresponding SEM image of $LiFePO_4$/yeast-20g L^{-1} (Fig.2c). It indicates that only Fe, O, P, C elements and no impurity are existed in the $LiFePO_4$/C composites, which keep in accordance with the evidence of XRD.

Fig.4. displays the TEM images of $LiFePO_4$/yeast-20g L^{-1}.Closer observations by TEM on morphology and structure of the $LiFePO_4$/C composites are gave in Fig.4a-d. The TEM observation confirms that the prepared $LiFePO_4$/C are nano-microspheres with lateral dimensions of ~300nm (Fig.4.a, b), which is in accordance with SEM images.

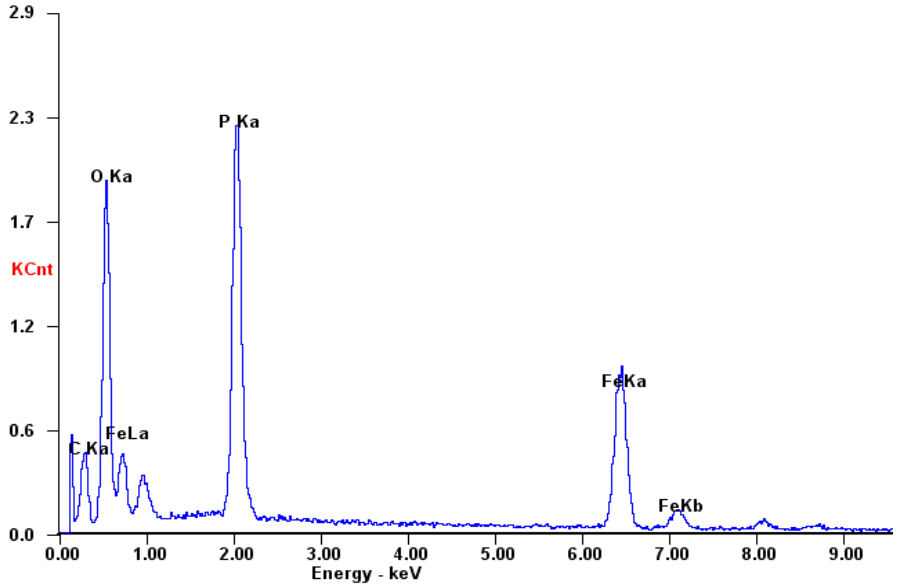

Figure 3. EDS spectra image of $LiFePO_4$/yeast-20 g L^{-1}

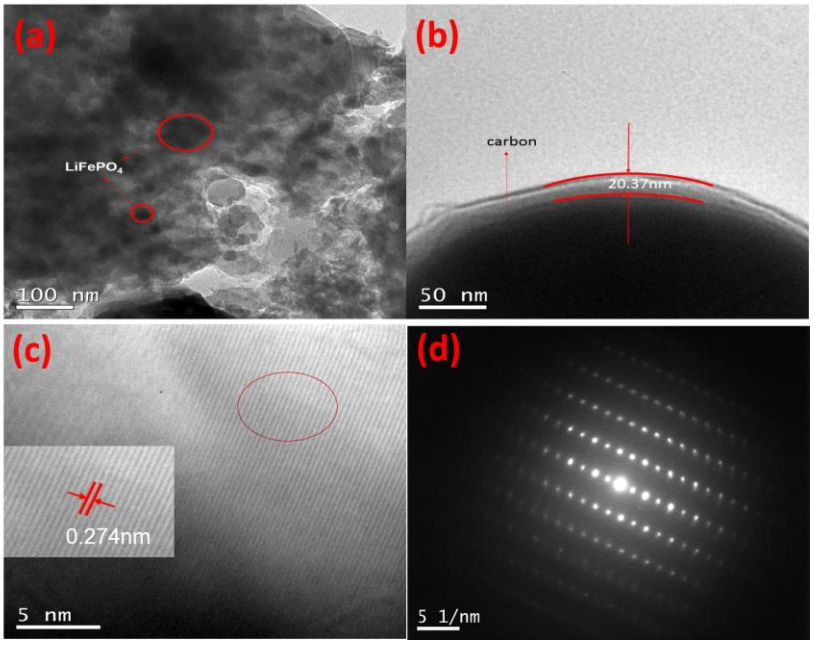

Figure 4. TEM images of $LiFePO_4$/yeast-20 g L^{-1} (a, b); (c, d) The magnified HR TEM images and SAED pattern of the partial area in (b);

Furthermore, the TEM images (Fig.4. b) further prove that carbon almost all tightly and homogeneous coated on the surface of $LiFePO_4$, and the carbon coating layers are about 20.37nm. The perfect carbon coating layers can effectively impede crystal and particle growth, as well as can enhance the ionic and electronic conductivity and stop corrosion of the electrode material [28]. The high-resolution TEM (HR-TEM) image (Fig.4. c) shows that set of lattices with interfringe spacing is 0.274nm. In addition, the spotted selected area electron diffraction (SAED) pattern demonstrates the single-crystalline orientation feature of the $LiFePO_4$/C (Fig.4. d).

Electrochemical performances are evaluated by galvanostatic charge/discharge measurements. Charge/discharge profiles at 0.1C are presented in Fig.5. Because of poor electrical conductivity, the $LiFePO_4$ composites without carbon coating ($LiFePO_4$/yeast-0g L^{-1}) exhibit the lowest discharge capacity (116.8mAh g^{-1}). Comparing with other curves, the sample that the additional amount of yeast cells is 20g L^{-1} shows the highest discharge capacities of 151.6mAh g^{-1}, and keeps the better discharge capacity of 147.8mAh g^{-1} (97.5% of its original value) after 50 cycles. Although the discharge capacity of the sample whose additional amount of yeast cells is 30g L^{-1} is close to the highest capacity in this graph, the discharge curve drops to 148.2mAh g^{-1} ahead of time. Comparing with other organic carbon source, $LiFePO_4$/C composites using yeast cells exhibit a higher discharge capacity [29-33]. This could be due to some factors, such as appropriate morphology of the microspheres, small particle size, uniform distribution and effectively carbon coating layer.

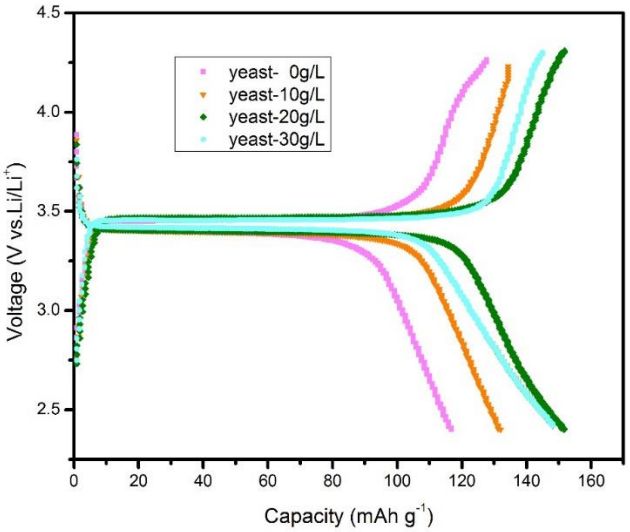

Figure 5. Charge/discharge curve at 0.1C of all samples: $LiFePO_4$/yeast-0g L^{-1}, $LiFePO_4$/yeast-10g L^{-1}, $LiFePO_4$/yeast-20g L^{-1}, $LiFePO_4$/yeast-30g L^{-1}

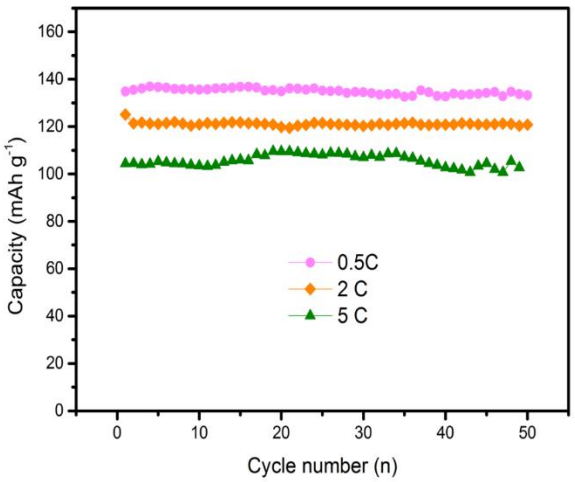

Figure 6. The cycling performances of $LiFePO_4$/yeast-20g L^{-1} at different rates: 0.5C, 2C, 5C

The cycling performance of the sample, which the amount of yeast cells is 20g L^{-1} at room temperature, is also interesting, as shown in Fig.6. It can be seen that the charge-discharge specific capacity have any remarkable reducing after 50 cycles at 0.5C and 2C rates. The discharge specific capacity at 5C has a slight fluctuation, but it does not reduce after 50 cycles. Apart from the confirmation of the superior performance, the plot provides evidence of the good cycling stability of this sample. During the process of lithium intercalation/deintercalation, a combination of polarizations, such as electrolyte polarization, electron-transfer resistance within the electrode, causes the overall cell-voltage [34]. Therefore, the reason may be caused by the particle size of $LiFePO_4$ that shorten the path of the transportation of lithium ion and reduce the polarization resistance from the process of electronic transfer [35-38].

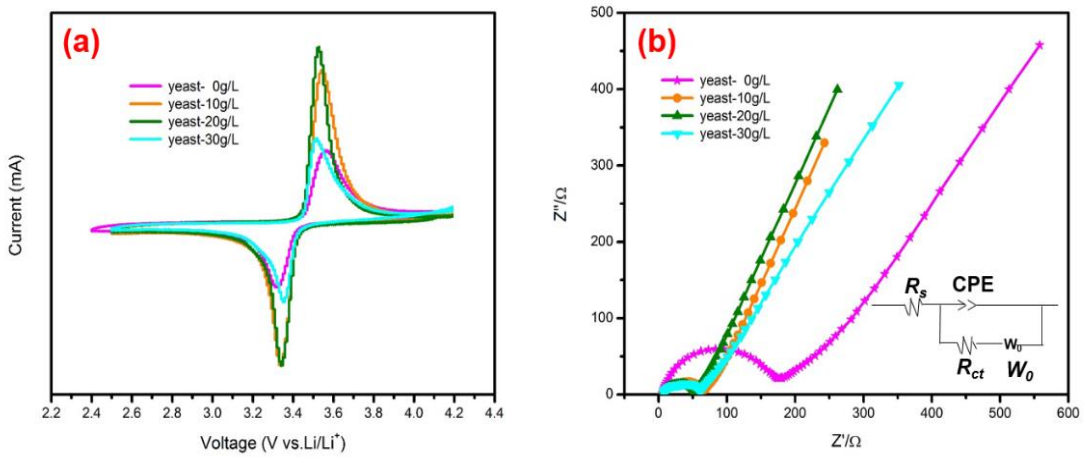

Figure 7. (a) CV determination of all samples: $LiFePO_4$/yeast-0g L^{-1}, $LiFePO_4$/yeast-10g L^{-1}, $LiFePO_4$/yeast-20g L^{-1}, $LiFePO_4$/yeast-30g L^{-1} at scan rate 0.1mV s^{-1}; (b) EIS measurement of all samples: $LiFePO_4$/yeast-0g L^{-1}, $LiFePO_4$/yeast-10g L^{-1}, $LiFePO_4$/yeast-20g L^{-1}, $LiFePO_4$/yeast-30g L^{-1}

As shown in the Fig.7.a, the CV curve of all $LiFePO_4$ materials are tested at a scan rate of 0.1mV s^{-1} from 2.4V to 4.2V (vs. Li/Li^+). The sample $LiFePO_4$/yeast-20g L^{-1} exhibits a couple of redox peaks between 3.34V to 3.53V, which indicates that the gain and the loss of electrons in the $LiFePO_4$ crystal structures are affected by Fe^{2+}/Fe^{3+} redox pair during the lithium insertion and extraction process [39]. On the contrast, the reduction and oxidation peaks of $LiFePO_4$/yeast-0g L^{-1} appears at 3.32V and 3.56V, $LiFePO_4$/yeast-10g L^{-1} appears at 3.33V and 3.53V, $LiFePO_4$/yeast-30g L^{-1} appears at 3.35V and 3.51V respectively. Comparing with other samples, the separation potential of $LiFePO_4$/yeast-20g L^{-1} is narrower and incisive. It is keeping with the galvanostatic charge/discharge curve (Fig.4.). From the Fig.5.b, a semicircle and a straight line in the high frequency region and low frequency region constitute the EIS curve. The charge-transfer resistance (R_{ct}) is indicated by semicircle and the inclined line is the Warburg Impedance (*Ws*) [40]. The resistance of the $LiFePO_4$/C electrode ($LiFePO_4$/yeast-20g L^{-1}) is much smaller than other samples. The tightly and uniform carbon coating layers have a great influence on impedance, which can enhance the electronic

conductivity. Therefore, it can be concluded that the uniform carbon coating via a bio-synthesis method is a benefit choice to improve the electrochemical performance of $LiFePO_4$/C.

4. CONCLUSIONS

In conclusion, high performance $LiFePO_4$/C nanocomposites have been prepared by an effective and controllable bio-synthesis method and the Baker's yeast cells are used as structural templates and biocarbon sources. This study discusses that the yeast cells impact on the electrochemical performance. The tests show that $LiFePO_4$/C with 20g L^{-1} yeast cells has the highest discharge specific capacity (151.6mAh g^{-1} at 0.1C) and good cycling stability, because of the small size of $LiFePO_4$/C particles and uniform carbon coating. This indicates that $LiFePO_4$/C nanocomposites via bio-synthesis method are an ideal type of cathode-active material for making high-power lithium ion batteries. Through biomimetic materials design, $LiFePO_4$ cathode material can meet the astringent requirements for high power applications.

ACKNOWLEDGEMENTS
This work was financially supported by the National Natural Science Foundation of China (No.11264023) and the Natural Science Foundation of Gansu Province, China (No. 1210ZTC035).

References

1. K. Fu, Y. Wang, C. Yan, Y. Yao, Y. Chen, J. Dai, S. Lacey, Y. Wang, J. Wan, T. Li, Z. Wang, Y. Xu and L. Hu, *Adv. Mater.*, 28 (2016) 2587–2594.
2. Z. Wu, S. Ji, T. Liu, Y. Duan, S. Xiao, Y. Lin, K. Xu and F. Pan, *Nano Lett.*, 16 (2016) 6357–6363.
3. R. Saroha, A. K. Panwar, Y. Sharma, P. K. Tyagi and S. Ghosh, *Appl. Surf. Sci.*, 394 (2017) 25–36.
4. A. Farmann, W. Waag and D. U. Sauer, *J. Power Sources*, 299 (2015) 176–188.
5. Z. Feng, L. Wang, Y. Wang, J. Chen, Z. He, D. Ji and Y.-X. Zhang, *J. Alloys Compd.*, 651 (2015) 712–717.
6. J. Manzi, M. Curcio and S. Brutti, *Nanomaterials*, 5 (2015) 2212–2230.
7. L. Oliveira, M. Messagie, S. Rangaraju, J. Sanfelix, M. Hernandez Rivas and J. Van Mierlo, *J. Clean. Prod.*, 108 (2015) 354–362.
8. B. Michalak, B. B. Berkes, H. Sommer, T. Bergfeldt, T. Brezesinski and J. Janek, *Anal. Chem.*, 88 (2016) 2877–2883.
9. E. Sarasketa-Zabala, E. Martinez-Laserna, M. Berecibar, I. Gandiaga, L. M. Rodriguez-Martinez and I. Villarreal, *Appl. Energy*, 162 (2016) 839–852.
10. K. Naoi, K. Kisu, E. Iwama, S. Nakashima, Y. Sakai, Y. Orikasa, P. Leone, N. Dupré, T. Brousse, P. Rozier, W. Naoi and P. Simon, *Energy Env. Sci*, 9 (2016) 2143–2151.
11. Z. Tian, S. Liu, F. Ye, S. Yao, Z. Zhou and S. Wang, *Appl. Surf. Sci.*, 305 (2014) 427–432.
12. C. Fasciani, S. Panero, J. Hassoun and B. Scrosati, *J. Power Sources*, 294 (2015) 180–186.
13. K. Zhang, J.-T. Lee, P. Li, B. Kang, J. H. Kim, G.-R. Yi and J. H. Park, *Nano Lett.*, 15 (2015) 6756–6763.
14. Y. Liu, J. Gu, J. Zhang, F. Yu, L. Dong, N. Nie and W. Li, *J. Power Sources*, 304 (2016) 42–50.
15. A. M. Bruck, C. A. Cama, C. N. Gannett, A. C. Marschilok, E. S. Takeuchi and K. J. Takeuchi, *Inorg Chem Front*, 3 (2016) 26–40.

16. Y. Liang, L. Chen, L. Cai, H. Liu, R. Fu, M. Zhang and D. Wu, *Chem Commun*, 2016, **52**, 803–806.
17. Y. Li, F. El Gabaly, T. R. Ferguson, R. B. Smith, N. C. Bartelt, J. D. Sugar, K. R. Fenton, D. A. Cogswell, A. L. D. Kilcoyne, T. Tyliszczak, M. Z. Bazant and W. C. Chueh, *Nat. Mater.*, 13 (2014) 1149–1156.
18. Y. Yao, P. Qu, X. Gan, X. Huang, Q. Zhao and F. Liang, *Ceram. Int.*, 42 (2016) 18303–18311.
19. B. Wang, B. Xu, T. Liu, P. Liu, C. Guo, S. Wang, Q. Wang, Z. Xiong, D. Wang and X. S. Zhao, *Nanoscale*, 6 (2014) 986–995.
20. T. Fan, B. Sun, J. Gu, D. Zhang and L. W. M. Lau, *Scr. Mater.*, 53 (2005) 893–897.
21. X. Zhang, X. Zhang, W. He, C. Sun, J. Ma, J. Yuan and X. Du, *Colloids Surf. B Biointerfaces*, 103 (2013) 114–120.
22. X. Du, W. He, X. Zhang, Y. Yue, H. Liu, X. Zhang, D. Min, X. Ge and Y. Du, *J. Mater. Chem.*, 22 (2012) 5960.
23. Y.-C. Chang, C.-Y. Lee and H.-T. Chiu, *ACS Appl. Mater. Interfaces*, 6 (2014) 31–35.
24. X. Zhang, W. He, Y. Yue, R. Wang, J. Shen, S. Liu, J. Ma, M. Li and F. Xu, *J. Mater. Chem.*, 22 (2012) 19948.
25. W. Li, J. Hwang, W. Chang, H. Setiadi, K. Y. Chung and J. Kim, *J. Supercrit. Fluids*, 116 (2016) 164–171.
26. C. Gong, Z. Xue, S. Wen, Y. Ye and X. Xie, *J. Power Sources*, 318 (2016) 93–112.
27. N. Bai, K. Xiang, W. Zhou, H. Lu, X. Zhao and H. Chen, *Electrochimica Acta*, 191 (2016) 23–28.
28. R. Wu, G. Xia, S. Shen, F. Zhu, F. Jiang and J. Zhang, *RSC Adv.*, 4 (2014) 21325.
29. Y.-C. Chang, C.-T. Peng and I.-M. Hung, *J. Mater. Sci.*, 49 (2014) 6907–6916.
30. P. M. Pratheeksha, E. H. Mohan, B. V. Sarada, M. Ramakrishna, K. Hembram, P. V. V. Srinivas, P. J. Daniel, T. N. Rao and S. Anandan, *Phys Chem Chem Phys*, 19 (2017) 175–188.
31. S. Qiu, X. Zhang, Y. Li, T. Sun, C. Wang and C. Qin, *J. Mater. Sci. Mater. Electron.*, 27 (2016) 7255–7264.
32. R. Scipioni, P. S. Jørgensen, D.-T. Ngo, S. B. Simonsen, Z. Liu, K. J. Yakal-Kremski, H. Wang, J. Hjelm, P. Norby, S. A. Barnett and S. H. Jensen, *J. Power Sources*, 307 (2016) 259–269.
33. O. Y. Posudievsky, O. A. Kozarenko, V. S. Dyadyun, V. G. Koshechko and V. D. Pokhodenko, *J. Solid State Electrochem.*, 19 (2015) 2733–2740.
34. S. W. Oh, H. J. Bang, S.-T. Myung, Y. C. Bae, S.-M. Lee and Y.-K. Sun, *J. Electrochem. Soc.*, 155 (2008) A414.
35. W. Yang, J. Liu, X. Zhang, L. Chen, Y. Zhou and Z. Zou, *Appl. Energy*, 6 (2016) 047.
36. H. Liao, H. Zhang, H. Hong, Z. Li, G. Qin, H. Zhu and Y. Lin, *J. Membr. Sci.*, 514 (2016) 332–339.
37. W. C. Chueh, F. El Gabaly, J. D. Sugar, N. C. Bartelt, A. H. McDaniel, K. R. Fenton, K. R. Zavadil, T. Tyliszczak, W. Lai and K. F. McCarty, *Nano Lett.*, 13 (2013) 866–872.
38. W. Feng, Y. Cao, X. Zhao, J. Gang and W. Su, *Int. J. Electrochem. Sci.*, (2017) 5199–5207.
39. H. Gong, H. Xue, T. Wang and J. He, *J. Power Sources*, 318 (2016) 220–227.
40. H. Shu, X. Wang, Q. Wu, B. Ju, L. Liu, X. Yang, Y. Wang, Y. Bai and S. Yang, *J. Electrochem. Soc.*, 158 (2011) A1448.